

A Comprehensive Design Methodology for Switched Reluctance Machines

M. N. Anwar, *Member, IEEE*, Iqbal Husain, *Senior Member, IEEE*, and Arthur V. Radun, *Senior Member, IEEE*

Abstract—The description of a comprehensive design methodology for switched reluctance machines (SRMs) is reported here. The magnetic properties of the iron, the number of phases, and the number of poles per phase all have a nonlinear effect on an SRM's performance. These effects, along with the sizing of the machine envelope and internal dimensions, make the machine design an insight-intensive effort. Maximization of torque density, power output, efficiency, speed range, and first critical speed and minimization of torque ripple, temperature rise, acoustic noise, and overall cost are among the many design objectives and critical issues that must be addressed during the design process. A design methodology that maximizes the desired features and minimizes the unwanted effects is presented here. Static and dynamic system-level simulations and finite-element analysis have been carried out for a four-phase 8/6 1.0-kW SRM as a design example to support the efficacy of the proposed design procedure.

Index Terms—Switched reluctance machines.

NOMENCLATURE

Dimensions,¹ Configuration, and Parameters

A_{pe}, A_{pm}	Electrical and mechanical area product, respectively.
A_{wn}, K	Net window area for each coil side and window factor.
A_{wire}	Cross-sectional area of each wire in the pole winding.
B_{sat}, g	Saturation flux density and air-gap length, respectively.
β_s, β_r	Stator and rotor pole-arc width for each repetition.
ΔT	Temperature rise halfway along the L_{stk} on the coil side.
$f_{m(=0,2,4)}$	Circumferential mode frequency for mode $m = 0, 2, \text{ and } 4$.

h_s, h_r	Stator and rotor pole height, respectively.
I_{plp}, J_{rms}	Peak phase current and rms current density, respectively.
K_L, S_{tf}	Inductance overlap ratio and stacking factor.
l_{r1}	Spacing between unaligned stator and rotor pole tips.
n_{ser}, n_{par}	Number of series and parallel paths in the winding.
N_{ph}, N_{rep}	Number of phases and repetition, respectively.
L_{stk}, N_p	Stack length and number of turns per pole, respectively.
n_c, P_{max}	First critical speed and maximum rated power.
P, Pf	Pole pitch = $\pi \cdot R_{out} \cdot N_{ph}^{-1} \cdot N_{rep}^{-1}$ and power factor.
R_{shft}, R_{ry}	Shaft radius and radius to rotor yoke, respectively.
R_g, R_{sy}	Radius to rotor pole tips and the radius to stator yoke.
R_{out}, R_{ph}	Machine outer radius and resistance of each phase.
ρ_m, T_s	Material density and hoop stress, respectively.
$T_{e\rho}, T_{rated}$	Maximum rotor torque density and rated torque.
t_s, t_r	Stator and rotor lateral pole width, respectively.
θ_c^λ	Critical rotor position for flux density.
θ_c^i	Critical rotor position for current.
W_t, V_{bus}	Total weight of the machine and bus voltage.
$\omega_b, \omega_{mrated}$	Base and maximum rated speed of the machine.
y_s, y_r	Thickness of the stator and rotor yoke, respectively.
α_{rms}	Ratio of rms to peak phase currents.
α_u	Ratio of unaligned to aligned flux linkage.
η	Efficiency of the machine.

Design Ratios

$\alpha_{hrtr1}, \alpha_{hrhs}, \alpha_{gyrs}$	Ratios of h_r/l_{r1} , h_r/h_s , and y_r/y_s , respectively.
$\alpha_n, \alpha_{RgRout}, \alpha_{tsP}$	Ratios of y_s/t_s , R_g/R_{out} , and t_s/P , respectively.

I. INTRODUCTION

THE switched reluctance machine (SRM) is a viable contestant for a number of applications that require high reliability, wide speed range at constant power, low manufacturing cost, and fast dynamic response. Like all other machines, the SRM has a unique set of characteristics that make it suitable for certain applications and unsuitable for others. The degree of suitability of an SRM for any application depends on the application's requirements and objectives. The specific weighting

Paper IPCSD 01-052, presented at the 2000 Industry Applications Society Annual Meeting, Rome, Italy, October 8-12, and approved for publication in the IEEE TRANSACTIONS ON INDUSTRY APPLICATIONS by the Electric Machines Committee of the IEEE Industry Applications Society. Manuscript submitted for review May 1, 2000 and released for publication August 6, 2001. This work was supported by the National Science Foundation under Grant ECS9702370 and by an Ohio Board of Regents Individual Research Challenge Award.

M. N. Anwar was with the Department of Electrical Engineering, The University of Akron, Akron, OH 44325-3904 USA. He is now with the Advanced Powertrain Engineering Group, Visteon Corporation, Dearborn, MI 48120 USA (e-mail: manwar9@visteon.com).

I. Husain is with the Department of Electrical Engineering, The University of Akron, Akron, OH 44325-3904 USA (e-mail: ihusain@uakron.edu).

A. V. Radun is with the Department of Electrical Engineering, University of Kentucky, Lexington, KY 40506-0046 USA (e-mail: radun@engr.uky.edu).

Publisher Item Identifier S 0093-9994(01)09700-6.

¹Dimensions are shown in Fig. 2.

of the numerous design objectives, common to all applications, is application specific. Therefore, various objectives need to be compromised to achieve an optimal design. Various SRM design aspects have been studied and reported in the literature [1]–[4], emphasizing the parameters, the number of phases, the number of machine repetitions, and a few design ratios (the ratios between various internal dimensions of the machine). However, a comprehensive design methodology is nonexistent in the literature. The present research describes a design methodology and sets design guidelines to encompass the effects of machine geometry, configuration, and parameters on the overall performance of the SRM. Torque ripple, acoustic noise, and wide speed range are considered as critical issues during the design process. The existing body of SRM design knowledge has been utilized whenever possible. The proposed methodology has been applied to design a four-phase 8/6 (single repetition) 1.0-kW SRM. The overall performance of the designed SRM has been verified with static and dynamic system-level simulations. Finite-element analysis (FEA) has also been carried out to verify the static characteristic curves of flux linkage and torque.

II. DESIGN METHODOLOGY

A. Design Steps

Fig. 1 shows a comprehensive flowchart describing the design steps that constitute the SRM design methodology. These steps include the initial selection of the SRM configuration, parameters and design ratios, validation of an “output checklist,” verification of overall performance, and FEA. The design specifications may include all or some of T_{rated} , ω_b , ω_{mrate} , P_{max} , Pf , V_{bus} , I_{php} , torque ripple, acoustic noise, and ambient temperature, depending on the application. The selection of configuration encompasses selecting N_{ph} , N_{rep} , n_{ser} , and n_{par} . The parameters T_s , $T_{e\rho}$, J_{rms} , and B_{sat} are the major contributors to the envelope sizing and temperature rise of the machine. The design ratios are associated with specific requirements of mean torque, torque ripple, acoustic noise, and efficiency.

Although a complex SRM model [5] is used for static and dynamic performance analysis, simplified output equations are used for the initial sizing and “output checklist” to simplify the back and forth adjustment of the design variations. Configuration, parameters, and design ratios are changed within their own limits to obtain a satisfactory “output checklist” for the design. In the next step, static and dynamic performance of the candidate design are verified, ultimately using FEA, to check whether the critical machine parameters meet their requirements. The design steps are continued in an iterative manner until the design requirements are met. Most of the design iterations fall within the shaded blocks shown in Fig. 1, where the forward and backward design equations and guidelines are used.

Other inputs to the design process are the design ratios in the Nomenclature. These design ratios are ultimately determined by a combination of experience and more detailed analysis, some of which is given below and some of which is in the literature [5]–[12].

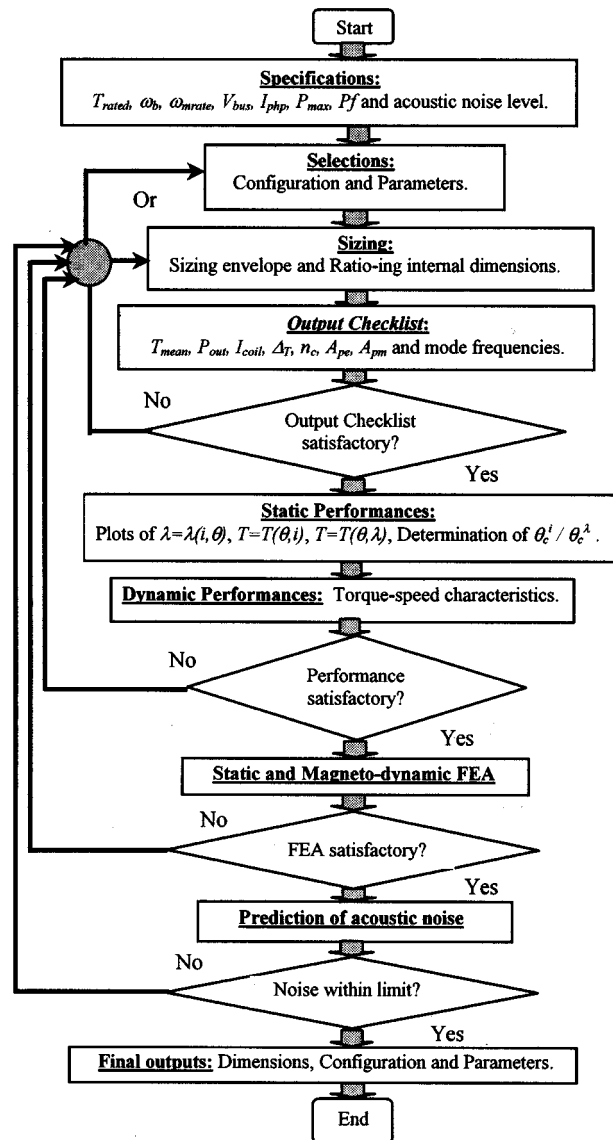


Fig. 1. Flowchart of the overall design methodology of SRM.

B. Specifications for a Design Example

A four-phase 8/6 1.0-kW SRM is to be designed for an application requiring minimum acoustic noise, wide speed range operation, and minimum torque ripple. The specifications and torque–speed requirements for this design example are given in Table I. The general geometry of the machine is shown in Fig. 2. All of the plots given in the following sections are for this design example.

III. SELECTION OF PARAMETERS AND CONFIGURATION

A. Hoop Stress and Critical Speed

The concentrated stress due to a hole in a plane sheet is called the hoop stress. The rotor lamination ring can be treated as a plane sheet having a hole in the middle. The centrifugal forces at extremely high speed cause hoop stress in the rotor yoke. This is a tensile stress in a direction tangential to the circumference of the lamination ring to resist the strain causing the ring to lift off the shaft as shown in Fig. 3. During the design, it must be

TABLE I
SPECIFICATIONS OF THE FOUR-PHASE 8/6 DESIGN EXAMPLE SRM

Speed (rad/sec and (rpm))	Torque (N.m)	Battery specifications	Dimensions & Temperature
0	3.0	Supply voltage	$L_{stk} = 0.0508$ m and
$\omega_b = 157.1$ (1500)	3.0	$V_{bus} = 42$ volts;	$R_{out} = 0.0381$ m.
261.8 (2500)	2.5	Battery current	
523.6 (5000)	1.5	$I_{php} \leq 40$ amps and	
$\omega_{mrate} = 837.76$ (8000)	0.5	Total external	All at ambient
1570.8 (15000)	0.1	resistance = 0.1 Ω .	temperature 90° C.

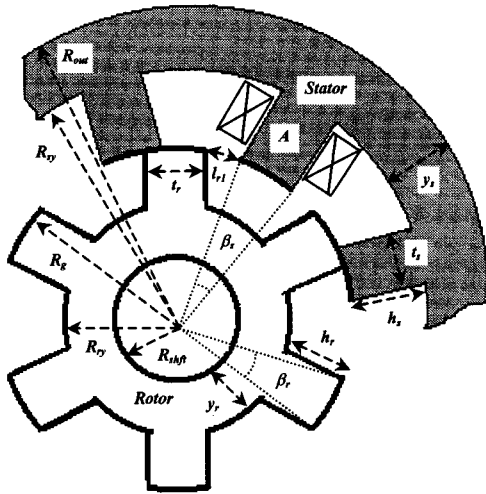


Fig. 2. A four-phase 8/6 SRM geometry where the rotor poles are in unaligned position with phase A.

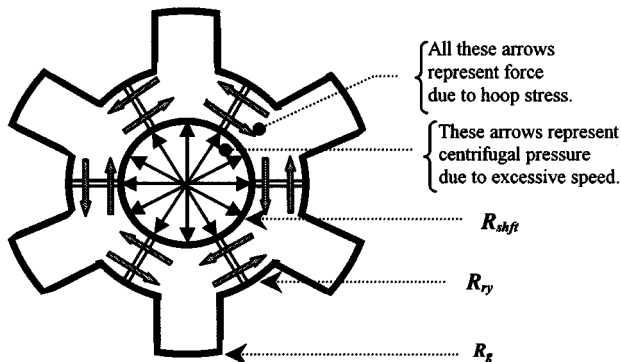


Fig. 3. Rotor lamination ring of a four-phase 8/6 SRM showing hoop stress.

insured that the hoop stress generated in the rotor lamination rings is sufficiently less than the rotor iron's yield strength. The rotor hoop stress T_s and maximum rated speed ω_{mrate} of the machine determine the maximum allowed value of R_g as

$$R_g = \frac{1}{\omega_{mrate}} \sqrt{\frac{T_s}{K_h}}. \quad (1)$$

The hoop stress constant K_h is a function of the material density, its Poisson's ratio, and some design ratios [5].

The rotor's first critical speed n_c is higher with larger R_{shft} and with lower rotor weight and stack length, because they maximize the lateral stiffness of the rotor [6]. This speed is to be kept well above the maximum rated speed. Fig. 4 shows R_g , L_{stk} , the product of R_g and L_{stk} (rotor envelop dimen-

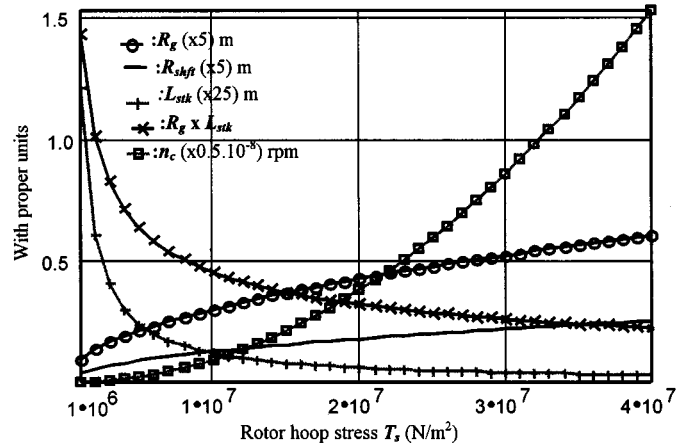


Fig. 4. Plots of R_g , L_{stk} , product of R_g and L_{stk} , R_{shft} and n_c with T_s .

sions), R_{shft} , and n_c as a function T_s when other parameters (ω_b , P_{max} , T_{rated} , A_{pm} , A_{pe} and A_{wn}) remain constant. From these plots, it is clear that envelope dimensions and volume of the machine decrease as T_s increases. It can be shown that the rotor power density increases as the square root of the rotor iron's yield strength [5]. Because the rotor envelope ($R_g \times L_{stk}$) decreases more slowly as T_s is increased beyond a certain limit, it is possible to design a high-speed high-power machine by increasing L_{stk} and decreasing R_g for a reduced rotor hoop stress. The setting of the value of T_s depends on the design tradeoff between the rotor envelope dimensions and the first critical speed in order to optimize the operating speed and the power density.

Once all of the SRM dimensions have been chosen, the effective hoop stress T_{eh} can be recalculated in the "output checklist" as

$$T_{eh} = \frac{\rho_m \cdot \left[2(R_g - R_{ry}) \cdot R_g \sin\left(\frac{\beta_r}{2}\right) + \frac{\pi}{N_{rep}} (R_{ry}^2 - R_{shft}^2) \right]}{4 \cdot \cos\left(\frac{\pi}{2 \cdot (N_{ph} - 1)N_{rep}}\right) \cdot y_r \cdot (R_g + R_{shft})^{-1} \cdot \omega_{mrate}^{-2}}. \quad (2)$$

To ensure that the hoop stress of the designed machine is within limit, the value of T_{eh} from (2) should be less than or equal to the initial hoop stress T_s used in (1).

B. Rotor Torque Density

An important parameter is the rotor torque density T_{ep} (torque per unit rotor volume), which depends strongly on the B_{sat} of the iron used. Because T_{ep} depends on the type of enclosure and the cooling process employed in a particular application, its value can vary from 2.5 kN·m/m³ to 250 kN·m/m³ [6]. Without any forced cooling, the value for T_{ep} is about 100 kN·m/m³ for SRMs employing cobalt-iron ($CoFe$) and 52 kN·m/m³ for SRMs using silicon-steel ($SiFe$). The rotor torque density varies inversely with the stack length as

$$L_{stk} = \frac{P_{max}}{\pi \cdot \omega_b \cdot R_g^2 \cdot T_{ep}}. \quad (3)$$

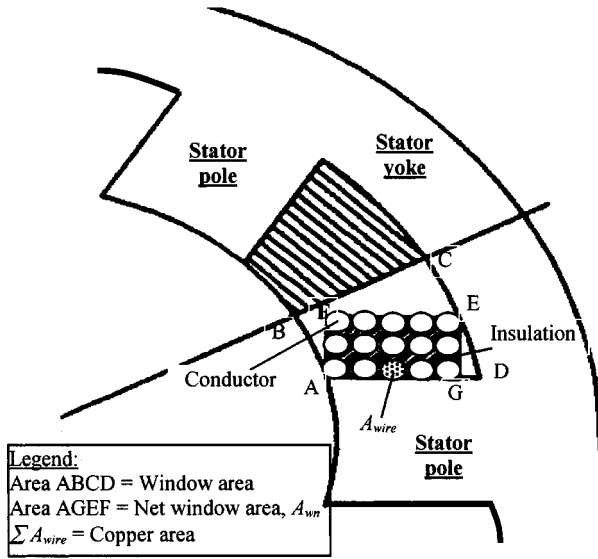


Fig. 5. Partial cross-sectional view of two adjacent stator poles showing the slot fill for phase windings.

In the design iterations of Fig. 1, the value of the mean rotor torque density T_{density} recalculated by (4) should be greater than or equal to $T_{e\rho}$

$$T_{\text{density}} = K_t \cdot \frac{J_{\text{rms}} \cdot A_{\text{wn}} \cdot B_{\text{sat}} \cdot S_{tf} \cdot n_{\text{ser}} \cdot n_{\text{par}}}{R_g} \quad (4)$$

K_t is a constant containing the ratios between the peak and rms values of phase current and torque, given by

$$k_t = \frac{\text{Peak phase current/Rms phase current}}{\pi \cdot \text{Peak phase torque/Average total torque}}$$

The peak to rms ratios are determined from detailed simulations of the proposed design. The constant k_t does not have a large variation and is typically equal to about 0.59.

C. RMS Current Density in the Coils

The rms current density J_{rms} is an important design parameter that affects a number of design outputs. The area products A_{pm} and A_{pe} , representing mechanical and electrical loading of the machine, obey the design constraint $A_{\text{pm}} \geq A_{\text{pe}}$ [5]. The expressions for these area products are

$$A_{\text{pe}} = \frac{8 \cdot \pi \cdot \alpha_{\text{rms}} \cdot P_{\text{max}}}{S_{tf} \cdot (1 - \alpha_u) \cdot P_f \cdot \eta \cdot B_{\text{sat}} \cdot J_{\text{rms}} \cdot K \cdot \omega_b} \quad (5)$$

$$A_{\text{pm}} = 4\pi \cdot R_g \cdot L_{\text{stk}} \cdot N_{\text{rep}} \cdot N_{\text{ph}} \cdot A_{\text{wn}} \quad (6)$$

Fig. 5 defines the net window area A_{wn} and the window factor K , which is the ratio between the window area and the copper area. The stacking factor S_{tf} is the ratio between actual stator length and the effective length of the iron. The actual length of the stator is greater than the length of the iron due to space between the stacked laminations and the insulation (often oxide) on the laminations.

The efficiency η used in (5) to calculate A_{pe} accounts for the iron loss of the machine. If the iron loss is high, the efficiency becomes low and, consequently, A_{pe} increases. This eventually will require a higher machine geometry to fulfill the

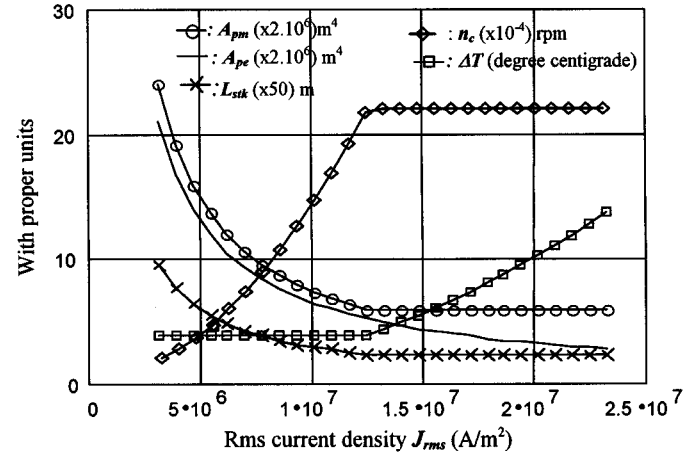


Fig. 6. Plots of A_{pe} , A_{pm} , L_{stk} , and ΔT with rms current density J_{rms} .

design constraint of $A_{\text{pm}} \geq A_{\text{pe}}$. Fig. 6 shows the effect of J_{rms} on L_{stk} , A_{pm} , A_{pe} , ΔT , and n_c . In this figure, the parameters T_s , $T_{e\rho}$ and the ratio of iron to copper area in the windows are held constant. The value of L_{stk} must satisfy both the back electromotive force (BEMF) and maximum torque density requirements of the machine. The value for A_{pm} is always higher than A_{pe} , for any value of L_{stk} [5]. However, A_{pm} starts diverging from A_{pe} when L_{stk} attains its minimum value and the critical speed n_c reaches its maximum. For an optimal utilization of mechanical and electrical loading of the geometry, J_{rms} is chosen to be somewhere near this divergence subject to the constraint that J_{rms} is not so large as to cause excessive copper losses. The values for optimal A_{pe} and A_{pm} are determined by trial and error to get the required machine performance. Fig. 6 also shows the dependence of the allowable maximum rms current density on ΔT , which is a function of thermal conductivity of the coil sides, shape of the conductor, and cooling process of the wires [6]. If the rise of ΔT above the ambient is higher than the insulation limit, the loading inequality $A_{\text{pm}} \geq A_{\text{pe}}$ is maintained by increasing the SRM's envelop dimensions by decreasing J_{rms} in the coils.

The other parameters associated with J_{rms} are the mean torque density T_{density} , the number of turns N_p , and the peak phase current I_{plp} . The variations of these parameters with J_{rms} are shown in Fig. 7, where the window areas of coil sides have been kept fixed. As expected, T_{density} increases with an increase in J_{rms} . Although I_{plp} remains the same, N_p must increase to maintain higher ampere-turns (magnetomotive force) with the increase of J_{rms} . With a lower J_{rms} , T_{density} as well as mean rotor torque are maintained by increasing the envelope dimensions without violating the loading inequality constraint.

D. Number of Phases and Poles per Phase

The selection of N_{ph} and N_{rep} depends primarily on the application. The multiplicity of the basic SRM configuration N_{rep} is equal to the number of pole pairs per phase. N_{ph} and N_{rep} together set the numbers of stator and rotor poles. Having a higher number of rotor poles gives a smaller stroke angle and leads to lower torque ripple at the cost of a decreased saliency ratio (ratio

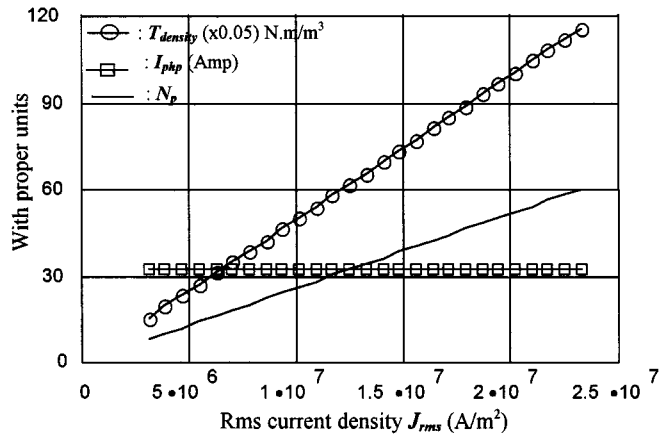


Fig. 7. Plots of $T_{density}$, I_{php} and N_p with rms current density J_{rms} .

between the maximum and minimum inductance levels). The decrease in saliency ratio will increase the controller volt-amperes and decrease the torque output. The number of strokes per revolution can be increased with a higher number of phases to alleviate the problem of torque dips with a smaller penalty in the saliency ratio [6]. Because of the lower torque dips, the average torque of the machine will increase. It would appear that doubling N_{rep} (while other parameters are held constant with all the coils of each phase connected in series) doubles the angular rate of change of phase flux, resulting in doubled torque at a given speed and current since the maximum and minimum inductances are unchanged. However, to a first order the total torque does not depend on the number of repetitions because N_p will have to be halved to keep the BEMF the same when N_{rep} is doubled. Further consideration of the rate of change of flux linkage, available coil area, saliency ratio, split ratio (α_{RgRout}), variation in the magnetic circuit reluctance, saturation behavior, and the iron loss due to the increase of the repetition modifies this simplistic conclusion. Doubling the number of repetitions will not contribute to the mean torque produced unless the pole width is made more than 50% of that for a single repetition machine. To maximize the co-energy both under high- and low-current conditions, the optimized stator pole width for a two-repetition machine is found to be approximately 70% of that of the single-repetition one [3]. This gives about 40% more thermally limited torque and horizontal force for the same copper loss and active volume. The above dependency of mean torque and torque dip with N_{ph} and N_{rep} can be explained with K_L , which is the ratio of inductance overlap of two adjacent phases to the angle over which the inductance is changing [1]. Equation (7) and Fig. 8 together define K_L

$$K_L = 1 - \frac{\text{Stroke Angle}}{\min(\beta_s, \beta_r)}$$

where

$$\text{Stroke Angle} = \frac{\pi}{N_{ph} \cdot N_{rep} \cdot (N_{ph} - 1)}. \quad (7)$$

The rotor pole arc β_r can be made slightly larger than the stator pole arc β_s to accommodate some of the fringing stator fluxes. However, making either the rotor or stator poles wider

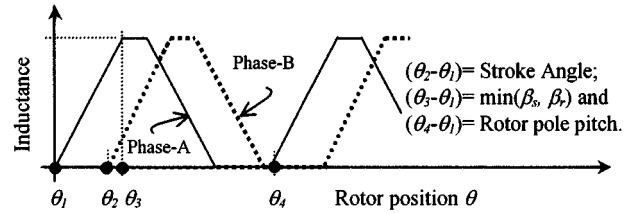


Fig. 8. Variation of phase inductance with rotor position.

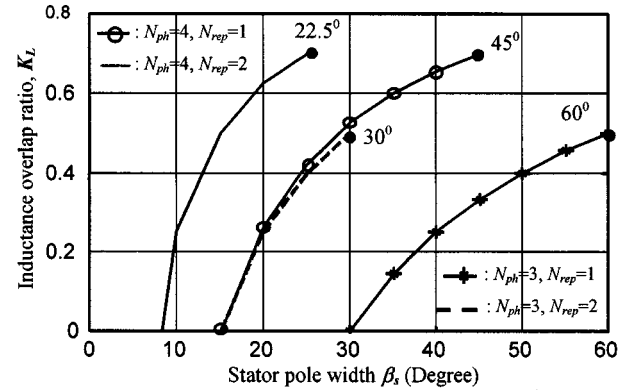


Fig. 9. Inductance overlap ratio versus stator pole width.

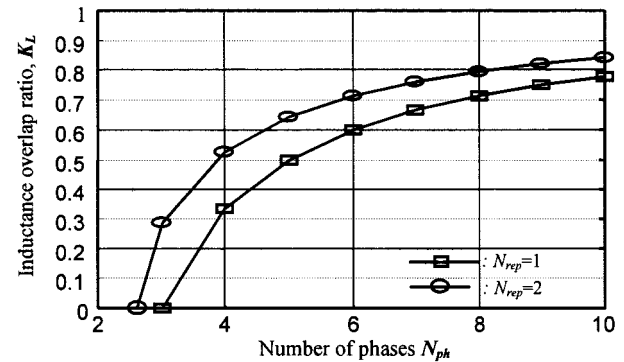


Fig. 10. Inductance overlap ratio versus number of phases.

than the other takes torque away from the aligned position. When one pole is wider than the other, there is a region around the aligned position where the stored energy (and inductance) does not change and, thus, the torque is zero. Thus, the pole arcs should be wide enough to insure that there is torque production for all rotor positions. Figs. 9 and 10 plot K_L versus β_s (assuming $\beta_s \leq \beta_r$) and K_L versus N_{ph} (assuming β_s for $N_{rep} = 2$ to be 70% of that of β_s for $N_{rep} = 1$). The higher the K_L , the lower will be the torque dip and the higher will be the mean torque as well. Fig. 9 shows that the minimum stator pole widths to start the machine (for $K_L \geq 0$) are approximately 10° and 30° for a “ $N_{ph} = 4, N_{rep} = 2$ ” and a “ $N_{ph} = 3, N_{rep} = 1$ ” machine, respectively. Therefore, it can be concluded that higher values of K_L are achievable at relatively low values of β_s for a machine with more phases and/or repetitions. These same machines have better starting capabilities. Figs. 9 and 10 also show that the improvement upon the problem of torque dip is noticeable in the lower range of β_s and lower N_{ph} . Thus, the number of phases or the

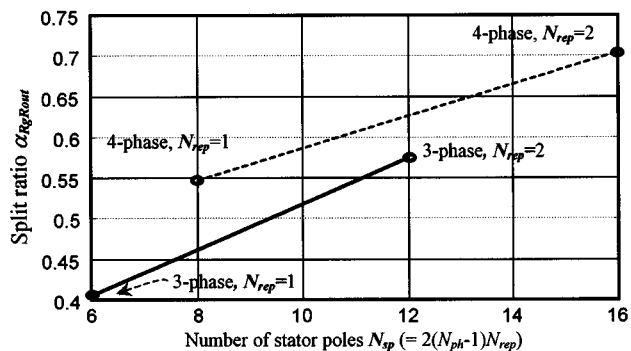


Fig. 11. Variation of split ratio with the change of N_{ph} and N_{rep} .

stator pole width should not be increased too much, since an increased number of phases increases the converter cost and an increased stator pole width decreases A_{wn} .

Another perspective on selecting N_{ph} and N_{rep} is that the increase in N_{ph} and N_{rep} requires a smaller pole width and, thus, a smaller stator back-iron width. Consequently, α_{RgRout} can be increased as shown in Fig. 11 while keeping the other design ratios and envelope dimensions constant. A higher α_{RgRout} provides space for a larger rotor diameter within the given frame size, which, in turn, produces more torque.

The higher the N_{rep} and N_{ph} of the machine, the less time there is available for the rise and fall of the phase currents. It is true that if N_{ph} or N_{rep} is doubled, the time for the phase current to rise is halved; fortunately, the current to be reached is also halved. Thus, unless the inductance has increased, there will no change in the total power due to all of the phases. It turns out that the BEMF does not depend on the pole width so that the total number of turns is the same (N_p decreases if pole windings are in series), even if N_{ph} is doubled. The unaligned inductance stays the same then because the path length halves, but so does the area of the coil sides. The two effects cancel leaving the unaligned inductance the same since the number of turns are the same. Thus, there is no more difficulty reaching the required (1/2) phase current with twice as many phases or repetitions if and only if the pole width with twice as many stator poles is halved. If the pole width has not been halved for the two-repetition machine, then it is harder to get the current into the machine and lower performance results.

Machines with $N_{rep} = 2$ have shorter flux paths, which reduce the core losses and the absorption of magnetomotive force (MMF) in the stator yoke. Shorter paths are achieved by means of the winding configuration and the lamination geometry. A higher inductance ratio in machines with higher phase numbers is also advantageous for sensorless operation.

IV. SIZING OF ENVELOPE AND INTERNAL DIMENSIONS

A. Envelope Sizing

The selection of envelope dimensions (R_g and L_{stk}) is governed by (1)–(6) in Section III. All other stator and rotor dimensions are determined as functions of R_g and the following four basic design ratios.

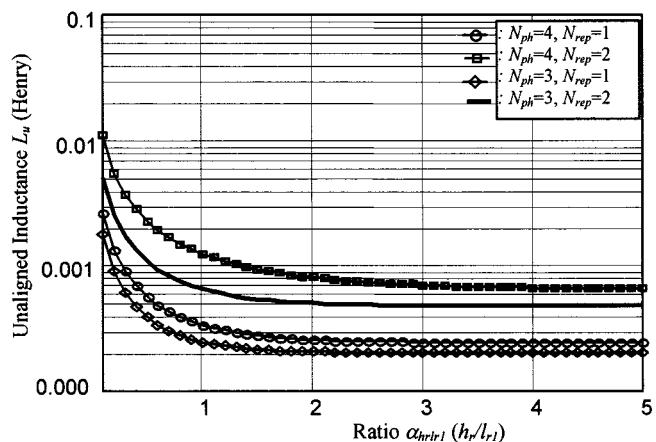


Fig. 12. Unaligned inductance versus the ratio α_{hrtr1} .

TABLE II
LIST OF FOUR BASIC DESIGN RATIOS FOR THREE- AND FOUR-PHASE SRMs

Design Ratios	$N_{ph}=4, N_{rep}=1$	$N_{ph}=4, N_{rep}=2$	$N_{ph}=3, N_{rep}=1$	$N_{ph}=3, N_{rep}=2$
α_{hrtr1}	2.0~2.5	2.5~3.0	1.5~2.0	2.0~2.5
α_{hrhs}	0.65~0.7	0.65~0.7	0.65~0.7	0.65~0.7
α_n	0.5~0.67	0.5~0.67	0.5~0.67	0.5~0.67
α_{yrys}	0.75~0.85	0.75~0.85	0.75~0.85	0.75~0.85

B. Design Ratios

The design ratios are defined to be the ratios between various internal dimensions of the machine. The objective functions of saliency ratio, unaligned inductance, torque, torque ripple, torque per ohmic loss, efficiency, acoustic noise, and torque–speed range [4]–[7] are taken into consideration in choosing the design ratios. A good understanding of the MMF profiles inside the machine geometry helps significantly in choosing the appropriate design ratios. The four basic design ratios are α_{hrtr1} , α_{hrhs} , α_n and α_{yrys} as defined in the Nomenclature.

The ratio α_{hrtr1} is chosen based on the desired saliency ratio and unaligned inductance L_u . Fig. 12 shows L_u versus α_{hrtr1} for 3 and 4-phase SRM's. The higher the ratio α_{hrtr1} , the lower is the L_u , which gives a higher saliency ratio. This ratio need not be greater than a certain maximum, since L_u levels off after that maximum. The objectives for selecting optimal values for α_n , α_{hrhs} and α_{yrys} are to maximize the stator mode frequencies, to minimize the envelope dimension (product of R_{out} and L_{stk}), to contain α_{RgRout} , α_{tsP} and α_{hrtr1} within limits and to insure a critical speed n_c well above the rated speed ω_{mrated} [7]. Table II gives a list of these design ratios for three- and four-phase SRMs.

C. Sizing h_r and h_s

The values of h_r and h_s are calculated using the following equation after choosing α_{hrtr1} and α_{hrhs} from Table II:

$$h_s = 2.R_g \cdot \frac{\alpha_{hrtr1}}{\alpha_{hrhs}} \cdot \sin \left(\frac{\pi}{4(N_{ph} - 1)N_{rep}} - \frac{\beta_r}{2} \right). \quad (8)$$

D. Sizing R_{out}

Outer radius R_{out} is calculated from R_g and h_s as

$$R_{\text{out}} = h_s + (R_g + g) \cdot \left(1 + 2 \cdot \alpha_n \cdot \sin \left(\frac{\beta_s}{2} \right) \right). \quad (9)$$

It is important to note here that, if a maximum R_{out} is given as a design constraint, the ratio $\alpha_{RgR_{\text{out}}}$ should be as high as possible to provide larger rotor diameter within the given frame to produce more torque. However, this will shrink the available window area for the windings, thus reducing the available MMF of the machine.

E. Sizing t_r and t_s

Dimensions t_r and t_s are the lateral length of the rotor and stator pole arcs, respectively. The rotor pole arc β_r should be slightly larger than the stator pole arc β_s to ensure the production of torque at all rotor positions without sacrificing the aligned inductance. This is achieved by allowing t_r to exceed t_s by a length between g and $2 \cdot g$ [6].

F. Sizing y_s and y_r

In an SRM with a two-pole flux pattern, the main flux divides into two equal parts when it leaves the poles and enters the yoke. Again, the sections of the yoke are shared between different overlapping phases, especially during high-speed operation. Hence, y_r and y_s should be more than 50% of t_r and t_s , respectively, to prevent back-iron saturation. The ratio of y_s over t_s (α_n) is also important from an acoustic noise point of view. The other consideration for choosing y_s is the machine weight limit. Dimension y_s is calculated as

$$y_s = R_{\text{out}} - \left[R_g + g + 2 \cdot R_g \cdot \frac{\alpha_{hrts}}{\alpha_{hrts}} \cdot \frac{\sin \left(\frac{\pi}{4(N_{\text{ph}} - 1)N_{\text{rep}}} - \frac{\beta_r}{2} \right)}{\cos \left(\frac{\beta_s}{2} \right)} \right]. \quad (10)$$

V. CRITICAL ISSUES

A. Acoustic Noise [7]

It is desirable to minimize the acoustic noise in SRM drives for many applications to avoid environmental noise pollution. The design objectives for noise reduction are to make the natural mode frequencies of the stator geometry as high as possible and to decrease the harmonic components of the magnetic radial force acting on the stator. A good design can be achieved if the dominant mode frequencies can be made higher than the audible range frequencies. The design ratios α_n and α_{hrts} , in Table II, need to be increased to have a thicker stator yoke to increase the mode frequencies. A thicker yoke reduces the SRM's power density, resulting in a lower utilization of the iron. Furthermore, if R_{out} is constrained, the net available window area

TABLE III
LIST OF α_n AND α_{hrts} FOR LOW ACOUSTIC NOISE SRM

Design Ratios	$N_{\text{ph}}=4, N_{\text{rep}}=1$	$N_{\text{ph}}=4, N_{\text{rep}}=2$	$N_{\text{ph}}=3, N_{\text{rep}}=1$	$N_{\text{ph}}=3, N_{\text{rep}}=2$
α_n	1.0~1.3	1.0~2.0	1.0~1.2	1.0~1.5
α_{hrts}	1.0~1.5	0.7~1.2	1.0~1.5	0.7~1.2

TABLE IV
DESIGN RATIOS α_{tsP} AND $\alpha_{RgR_{\text{out}}}$, TORQUE AS AN OBJECTIVE FUNCTION

Objective function	α_{tsP}	$\alpha_{RgR_{\text{out}}}$
Torque	0.27~0.47	0.57~0.63

for the windings decreases and the thermal diffusion distance for heat transfer from the windings to the outside frame increases. Therefore, the design choice for a low-noise machine requires a tradeoff among the desired quantities. The ranges for α_n and α_{hrts} , optimized for low acoustic noise design, are given in Table III.

The choice of the stator pole shape can play a small but effective role in reducing acoustic noise. A method known to be effective is to taper the stator pole from the top towards the air gap and to round the bottom of the slot. Analysis also shows that the greater the number of phases or repetitions, the lower the acoustic noise power level.

B. Torque Ripple

The application of an SRM in a servo system requires reduced torque ripples. One method of reducing torque ripple is to increase N_{ph} and N_{rep} , as explained in Section III-D. Increasing β_r and β_s also reduces torque deadband between adjacent phases and, thus, reduces torque ripples, assuming a suitable control design is used [2]. The dynamic torque ripples of the machine are reflected in the amount of torque dip found in the static plots of torque versus rotor position, as shown in Fig. 15. Reducing the torque dip may result in a lower mean torque, and a compromise solution must be sought. The ratios α_{tsP} and $\alpha_{RgR_{\text{out}}}$ should lie within the range given in Table IV [4] in order to maximize the mean torque. In the design iterations of Fig. 1, these two ratios are checked in the "output checklist" evaluation.

C. Wide Speed Range [8]

A wide speed range with adequate torque capability at higher speeds is desired in electric-propulsion-type applications. An SRM can satisfy this requirement only with efficient torque sharing between phases, which can be determined by two critical rotor positions. The critical rotor positions θ_c^i and θ_c^λ represent the two crossover angles where two neighboring phases produce equal values of torque at equal values of current and flux linkage, respectively. The design strategy is to extend these rotor positions, enabling the controller with dwelling flexibility. The SRM drive thus obtained will have wide speed range, lowered torque ripple, and extended constant-power range of operation. The higher the ratios α_{yry_s} and α_{hrts} , the wider is the separation between θ_c^i and θ_c^λ . The same objective can also be achieved by making the air-gap length as small as manufac-

TABLE V
DIMENSIONS, CONFIGURATION, PARAMETERS, AND SOME OUTPUTS
OF THE DESIGNED FOUR-PHASE 8/6 SRM

Dimensions (m)	Configuration/Parameters	Outputs
$L_{stk}=0.0508$; $R_{shaft}=0.009$; $R_{ry}=0.013$; $R_g=0.0203$; $R_{sy}=0.0305$; $R_{out}=0.038$ and $g=0.000254$ $\beta_s=22.5^\circ$; $\beta_r=22.8^\circ$	$n_{par}=1$; $n_{ser}=2$; $N_p=35$ $B_{sat}=1.8$ Tesla (M19 SiF _e) $A_{wire}=7.1 \cdot 10^{-7}$ m ² $W_r=1.135$ kg $\theta_c^\lambda = -13^\circ$; $\theta_c^i = -9^\circ$	$\Delta T=6.5^\circ$ C; $R_{ph}=0.3$ Ω ; $n_c=2 \cdot 10^5$ rpm; $f_{m(-0)} = 14200$ Hz $f_{m(-2)} = 1600$ Hz $f_{m(-4)} = 7961$ Hz Mean Noise=36.75 dB

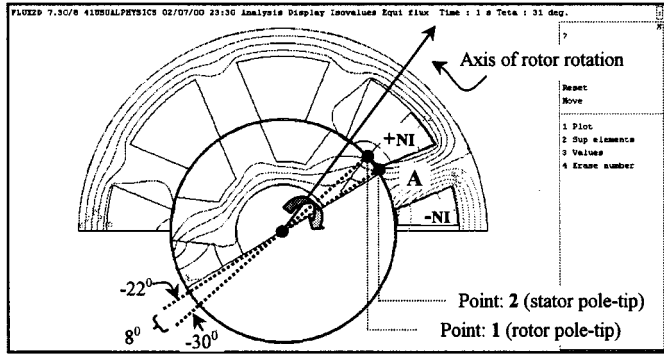


Fig. 13. Geometry of the designed four-phase 8/6 SRM.

turally possible. This criterion matches with the criteria to maximize the SRM's power density and torque density. Changing β_s , B_{sat} and N_p have conflicting effects on θ_c^i and θ_c^λ , which suggests that these parameters should be selected together in order to optimize the overall performance of the machine.

VI. FINAL OUTPUTS OF THE DESIGN EXAMPLE

The final results for the design example are summarized in Table V. This is a four-phase 8/6 (single repetition) 1-kW SRM as shown in Fig. 13.

A. Static Performances

Using the dimensions, configuration, parameters, and outputs from Table V, the static plots of flux linkage (λ) and torque (T) are checked to insure that they are satisfactory. Fig. 14 shows the λ - i - θ characteristic curves for the designed SRM calculated both by the analytical and the FEA methods. The maximum flux linkage at the pole-aligned position reaches a value of about 0.05 W at the maximum I_{php} of 40 A. This gives a saturation flux density of 1.89 T, whereas the B_{sat} for the M19 SiF_e used for this SRM is 1.8 T. Therefore, the machine geometry is utilizing the core material maximally up to its saturation level.

Fig. 15 shows the T - i - θ characteristic curves for the same SRM. Both the analytical and the FEA methods are employed to generate torque profiles for two adjacent phases. The maximum torque is about 3 N·m, which is sufficient to meet the torque requirement of the application.

The torque profiles of Fig. 15 show similar characteristics for the analytical and the FEA methods. The only significant difference in the characteristics is around the rotor position of -22° where rotor pole tip (point: 1) reaches stator pole tip (point: 2) as shown in Fig. 13. At this position, the effective air gap steps

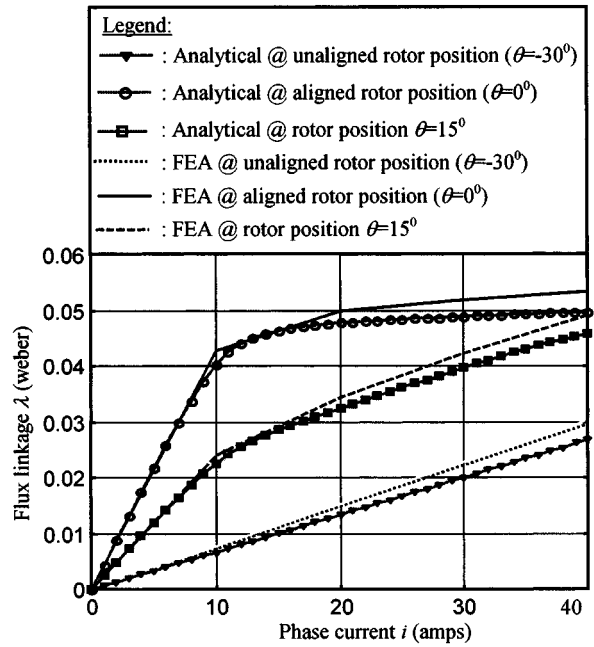


Fig. 14. Plots of flux linkage versus current for various rotor positions.

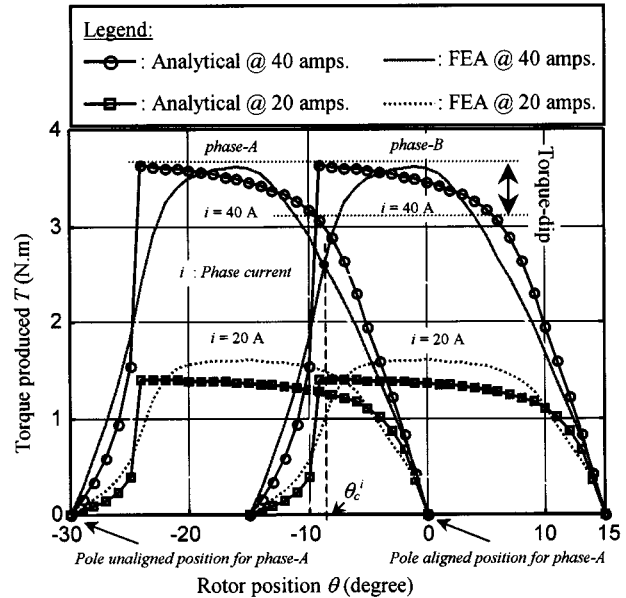


Fig. 15. Plots of torque versus rotor position for various current levels.

down from a higher value to g , which causes a discontinuity for the analytical calculation of static torque.

B. Dynamic Performance

System-level dynamic simulation to investigate the torque-speed characteristics of the designed SRM is done using the control algorithm described in [8]. The optimal phase commutation angle is varied from θ_c^i and θ_c^λ as a function of operating speed, torque, and phase current to maximize the torque-speed envelope. The computed torque-speed characteristic for the design example is shown in Fig. 16.

Comparing the torque-speed requirement in Table I and the computed characteristics in Fig. 16, it can be claimed that the

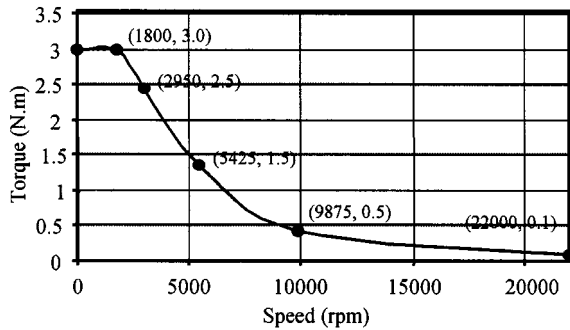


Fig. 16. Torque-speed characteristics of the designed SRM.

designed SRM is capable of handling the torque-speed requirements of the application.

VII. CONCLUSIONS

A comprehensive design methodology is presented in this paper. The use of the methodology is illustrated with a design example. The critical issues of torque ripple, acoustic noise, and wide speed range are addressed in the design process. The results establish design guidelines that encompass the effects of machine geometry, material properties, configuration, design parameters, and design ratios on the overall performance of the SRM.

Design examples with particular attributes, such as low acoustic noise design or wide speed range SRM design, are discussed in separate papers to provide sufficient details [7], [8]. Experimental verification of the design equations and methodology presented here appear in related publications [9], [10]. The calculations of various losses during design will be presented in a future paper.

REFERENCES

- [1] P. J. Lawrenson, J. M. Stephenson, P. T. Blenkinsop, J. Corda, and N. N. Fulton, "Variable-speed switched reluctance motors," *Proc. Inst. Elect. Eng.*, pt. B, vol. 127, no. 4, pp. 253–265, July 1980.
- [2] R. S. Wallace and D. G. Taylor, "Three-phase switched reluctance motor design to reduce torque ripple," in *Proc. 1990 Int. Conf. Electrical Machines*, Cambridge, MA, Aug. 1999, pp. 783–787.
- [3] H. C. Lovatt and J. M. Stephenson, "Influence of the number of poles per phase in switched reluctance motors," *Proc. Inst. Elect. Eng.*, pt. B, vol. 139, no. 4, pp. 307–314, July 1992.
- [4] J. Faiz and J. W. Finch, "Aspects of design optimization for switched reluctance motors," *IEEE Trans. Energy Conversion*, vol. 8, pp. 704–713, Dec. 1993.
- [5] A. V. Radun, "Design considerations for the switched reluctance motor," *IEEE Trans. Ind. Applicat.*, vol. 31, pp. 1079–1087, Sept./Oct. 1995.
- [6] T. J. E. Miller, *Switched Reluctance Motors and Their Control*. Oxford, U.K.: Clarendon, 1993.
- [7] M. N. Anwar and I. Husain, "Design perspectives of a low acoustic noise switched reluctance machine," presented at the IEEE-IAS Annu. Meeting, Rome, Italy, Oct. 2000.
- [8] —, "Design of a switched reluctance machines for wide speed range operation," presented at the ICEM, Espoo, Finland, Aug. 2000.
- [9] M. N. Anwar, I. Husain, and S. G. Kelly, "Effects of end-shield on the stator mode frequencies of electric machines," presented at the IEEE-IAS Annu. Meeting, Chicago, IL, Sept./Oct. 2001.

- [10] M. N. Anwar, I. Husain, S. Mir, and T. Sebastian, "Experimental evaluation of acoustic noise and mode frequencies with design variations of switched reluctance machines," presented at the IEEE-IAS Annu. Meeting, Chicago, IL, Sept./Oct. 2001.
- [11] A. V. Radun, "Analytically computing the flux linked by a switched reluctance motor phase when the stator and rotor poles overlap," *IEEE Trans. Magn.*, vol. 36, pp. 1996–2003, July 2000.
- [12] —, "Analytically calculating the SRM's unaligned inductance," *IEEE Trans. Magn.*, vol. 35, pp. 4473–4481, Nov./Dec. 1999.



M. N. Anwar (S'99–M'01) received the B. Sc. and M. Sc. degrees from Bangladesh University of Engineering and Technology, Dhaka, Bangladesh, and the Ph.D. degree from The University of Akron, Akron, OH, in 1994, 1995, and 2001, respectively, all in electrical engineering.

He is currently with the Advanced Powertrain Engineering Group, Visteon Corporation, Dearborn, MI. He was a Lecturer from 1994 to 1996, and an Assistant Professor from 1996 to 1997, at Bangladesh University of Engineering and Technology. His

research interests include design and modeling of electric machines, DSP-based control, and inverters for hybrid electric vehicle applications.



Iqbal Husain (S'89–M'89–SM'99) received the B.Sc. degree from Bangladesh University of Engineering and Technology, Dhaka, Bangladesh, and the M.S. and Ph.D. degrees from Texas A&M University, College Station, in 1987, 1989, and 1993, respectively, all in electrical engineering.

He is currently an Associate Professor in the Department of Electrical Engineering, The University of Akron, Akron, OH, engaged in teaching and research. He was a summer researcher for Wright Patterson AFB Laboratories in 1996 and 1997. Previously, he taught as a Lecturer at Texas A&M University and also was a Consulting Engineer for Delco Chassis, Dayton, OH. His research interests are in the areas of control and modeling of electrical drives, design of electric machines, and development of power conditioning circuits. He has worked extensively in the development of switched reluctance motor drives, including sensorless controllers.

Dr. Husain received the 2000 IEEE Third Millennium Medal and the 1998 Outstanding Young Member Award from the IEEE Industry Applications Society (IAS). He was also the recipient of two Prize Paper Awards from the Industrial Drives Committee of the IAS.



Arthur V. Radun (M'91–SM'95) received the Ph.D. degree from Massachusetts Institute of Technology, Cambridge, in 1981.

In 1981, he joined the General Electric Ordnance Systems Department, where he worked in the area of power electronics circuit design and electromagnet analysis. In 1996, he joined General Electric Corporate Research and Development, where he applied the latest power semiconductors to power control problems and worked on the development and application of switched reluctance motors to aircraft engine accessories.

Since 1993, he has been at the University of Kentucky, Lexington, where he is currently an Associate Professor of electrical engineering and has continued his power electronics research, including switched reluctance motor drive research. His research interests include solid-state power conditioning and motor drive development, control of power electronic systems, electromagnetics and electric machine development, and power semiconductor device physics.